Chapter 2
Angle-Resolved Photoemission Spectroscopy

2.1 Introduction

The macroscopic properties of solid materials are governed by their microscopic electronic structures, so it's important to study its electronic structure in order to understand, control or make use of the novel physics in various advanced materials. Electronic states in materials are reflected by the electron energy (E), momentum (**k**), and spin (**s**). ARPES is the sole technique that could probe all these physical quantities in solid materials, and this highly sophisticated experimental tool has played and irreplaceable role in the study of superconducting energy gap, pseudogap and many-body physics in cuprate high-temperature superconductors.

Much higher resolution and spin resolvable function of the ARPES technique are highly demanded in the study of condensed matters especially the cuprates superconductors of which the interested energy scale is tens of meV below Fermi level. The development of laser frequency doubling technology, especially the application of $KBe_2BO_3F_2$ recently [1], provided an opportunity to develop new generation of ARPES with ultra-high resolution [2]. After successfully building vacuum ultraviolet (VUV) laser-based ARPES system, based on the newly developed ultra-violet laser system, we designed and developed a spin resolved ARPES system with high energy resolution, a time-of-flight ARPES system and a photon energy tunable laser on the ARPES system. Figure 2.1 is the 3D simulated blueprint of the three ARPES systems in our lab. Based on the 3D modeling, we have completed the installation of the spin resolved ARPES and the time-of-flight ARPES system which will be introduced in this chapter in detail.

This chapter will mainly focus on three parts: (1) The principle of ARPES; (2) The development of VUV laser-based ARPES and (3) The development of spin resolved ARPES, time-of-fight ARPES and tunable laser-based ARPES.

2.2 The Principle of ARPES [3]

Photoemission experiments are based on photoelectric effect which was discovered by Hertz in 1887 [4] and fully explained by Einstein's photoelectric effect equation

W. Zhang, *Photoemission Spectroscopy on High Temperature Superconductor*, Springer Theses,
DOI 10.1007/978-3-642-32472-7_2, © Springer-Verlag Berlin Heidelberg 2013

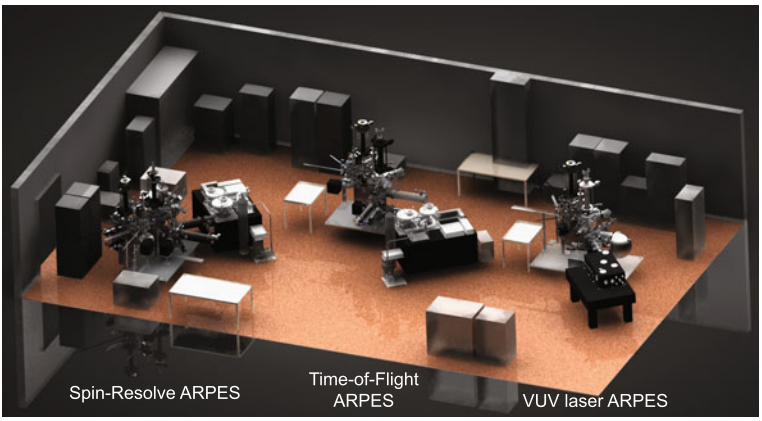

Fig. 2.1 The 3D modeling of the three distinctive ARPES system

in 1905 [5]. Based on the satisfaction of sudden [6] and adiabatic [7] approximation, photoelectron spectroscopy is a technique that probes the single-particle spectral function in solid materials directly.

2.2.1 Brief Description of ARPES

If the incident photon energy is higher than the work function of materials, electrons in the top several or tens of atom layers will be stimulated outside the material, and the energy of the outgoing photoelectrons could be calculated by the following equation [5]

$$E_{kin} = h\nu - \Phi - E_B \tag{2.1}$$

Usually, the work function in materials is 4∼5 eV so that the photon energy should be higher than 5 eV in photoemission experiments. Figure 2.2 shows the process of photoemission, and from which we can see that the density of states of outgoing electrons is proportional to that of the material. Because of the limited instrumental resolution and the bandwidth of incident photon energy, the density of states of outgoing electrons is broadened by convolving the resolution.

Figure 2.3 is a cartoon to show the process of the ARPES experiment. Photoelectrons are stimulated by incident photons and escape outside of material into the vacuum, and they are counted by an angle resolved electron energy analyzer. The momentum of photoelectrons could be calculated by

$$p = \sqrt{2mE_{kin}} \tag{2.2}$$

in which m is the mass of electron. The momentum components of parallel and perpendicular to sample surface are determined by the polar angle θ and azimuthal

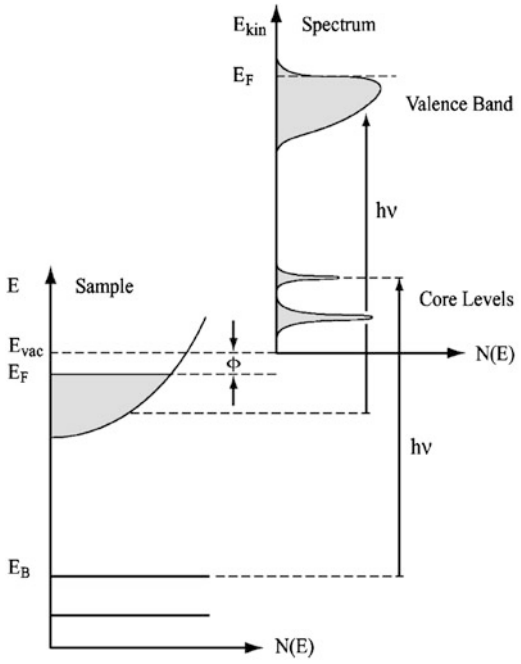

Fig. 2.2 The photoemission process. E_F, Fermi level; E_{vac}, vacuum level Φ, work function of sample; E_{kin}, kinetic energy of photoelectron; E_B, binding energy in material. Reprinted with permission from [3], copyright 2003, American Physical Society

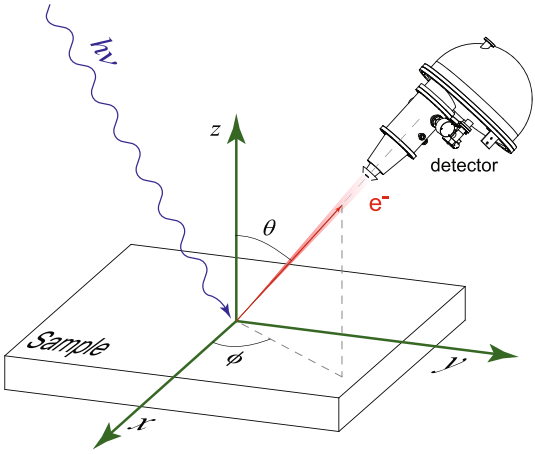

Fig. 2.3 Schematic of ARPES

angle ϕ of the sample. In the process of photoemission, total energy and momentum parallel to the surface are conserved, but the momentum perpendicular to the sample surface is not conserved because of the broken of translational symmetry along this direction. However, ARPES experiments mainly study two- or quasi two-dimensional systems in which there is little electronic dispersion perpendicular to the surface. For the light source (usually <1000 eV) used in ARPES experiments, the momentum of the photon is negligible comparing to that of electron, so the

energy and momentum of photoelectrons, binding energy (E_B) in solids, crystal momentum in solids ($\mathbf{K}$) could be related by

$$P_{\parallel} = \hbar K_{\parallel} = p \sin\theta = \sqrt{2mE_{kin}} \cdot \sin\theta \tag{2.3}$$

in which the $\hbar\mathbf{K}_{\parallel}$ is the component of electronic crystal momentum parallel to surface in the extended Brillouin zone. For large θ angle, the actual detection of the electron momentum may reach a high level of the Brillouin zone, and one can get reduced crystal momentum in the first Brillouin zone by subtracting the reciprocal lattice vector $\mathbf{G}$. Because of the broken of translational symmetry perpendicular to the sample surface, the momentum component in this direction couldn't be directly obtained from regular ARPES experiments. A special situation is that the electronic dispersion perpendicular to the surface is negligible in low-dimensional systems in which the electronic structure is usually strong anisotropic. In the case of cuprate superconductors, its electronic structure is almost two dimensional especially for Bi2212 in which electronic dispersion could be fully described by $\hbar\mathbf{K}_{\parallel}$.

It's worth noting that it's easy to get high energy and momentum resolution for low photon energy, and it's the case of ARPES experiments that usually use light source in the ultraviolet range $h\nu < 100$ eV. The momentum resolution $\Delta K_{\parallel}$ could be simply calculated from Eq. 2.3 that

$$\Delta K_{\parallel} \simeq \sqrt{2mE_{kin}/\hbar^2} \cdot \cos\theta \cdot \Delta\theta \tag{2.4}$$

where the item $\Delta\theta$ is the angular resolution of the detector. From Eq. 2.4, generally speaking, for certain angular resolution, a lower photon energy or large polar angle θ can give a better momentum resolution.

2.2.2 Single Particle Spectral Function

The process of photoemission is complicated from the viewpoint of quantum physics, and it's a single-step quantum mechanism event. To develop a formal description and due to the complexity of the one-step model [8–11], a phenomenological three-step model is introduced to describe the process of photoemission. Within the three-step model, the photoemission is subdivided into three independent steps [11–13],

1. Photon excitation of the electron in the solid.
2. Motion of the photoelectron to the surface.
3. Escape of the photoelectron into the vacuum.

However, the three-step model is just a phenomenological model, and it's easier to be understood. The details of the process of photoemission has been discussed in a book [14] and a review paper [3].

Actually, to deduce the electronic structure of solids from photoelectrons, sudden approximation should be satisfied [3, 14]. To make sure the photoelectrons carry the

information of the electronic structure of solids, one has to assume that the time of photoelectrons traveling from the bulk to vacuum is much shorter than recovery time of the transient electronic system after emitting electrons. Based on this approximation, one could deduce the momentum and energy of electrons in solids using momentum (Eq. 2.2) and energy (Eq. 2.1) conservations.

In quantum solid physics, the correlated electron system is usually described by Green's function formalism $G(\mathbf{k}, \omega)$ [15–18]. The single particle spectral function is the imaginary part of Green's function,

$$A(\mathbf{k}, \omega) = -\frac{1}{\pi} \operatorname{Im} G(\mathbf{k}, \omega) \tag{2.5}$$

The photoemission intensity as a function of energy and momentum of electrons at limited temperature could be written as

$$I(\mathbf{k}, \omega) = I_0(\mathbf{k}, \nu, \mathbf{A}) f(\omega) A(\mathbf{k}, \omega) \tag{2.6}$$

where the item $\mathbf{k} = k_\parallel$ is the inplane momentum of a quasi two dimensional system; ω is energy related to Fermi level; $I_0(\mathbf{k}, \nu, \mathbf{A}) \propto |M_{f,i}^{\mathbf{k}}|^2$ (matrix element item [3, 14]) is related to the momentum of electrons, the energy and polarization of incident photons; $f(\omega) = (e^{\omega k_B T} + 1)^{-1}$ is the Fermi-Dirac distribution function which confines the photoemission experiments that only occupied states could be probed. In actual experiments, limited energy and momentum resolution should be convolved into Eq. 2.6.

The interaction between electrons and other particles could be involved to Green's function by electron self-energy $\Sigma(\mathbf{k}, \omega) = \Sigma'(\mathbf{k}, \omega) + \Sigma''(\mathbf{k}, \omega)i$. The $\Sigma'(\mathbf{k}, \omega)$ and $\Sigma''(\mathbf{k}, \omega)$ are the real and imaginary parts of electron self-energy. The Green's function and single particle spectral function could be written as

$$G(\mathbf{k}, \omega) = \frac{1}{\omega - \varepsilon_{\mathbf{k}} - \Sigma(\mathbf{k}, \omega)} \tag{2.7}$$

$$A(\mathbf{k}, \omega) = -\frac{1}{\pi} \frac{\Sigma''(\mathbf{k}, \omega)}{[\omega - \varepsilon_{\mathbf{k}} - \Sigma'(\mathbf{k}, \omega)]^2 + [\Sigma''(\mathbf{k}, \omega)]^2} \tag{2.8}$$

By analyzing the photoemission spectra with spectral function in Eq. 2.8, the real and imaginary parts of electron self-energy could be extracted to study the many body interaction in solids, as discussed in following chapters.

2.3 Ultra-Violet Laser-Based ARPES

Most of the modern ARPES experiments are using synchrotron radiation light source or gas discharge light source. Lab based gas discharge lamp usually has a energy resolution around 1 meV (1.2 meV for helium discharge lamp), but the photon flux is not enough for energy analyzer working under high energy resolution

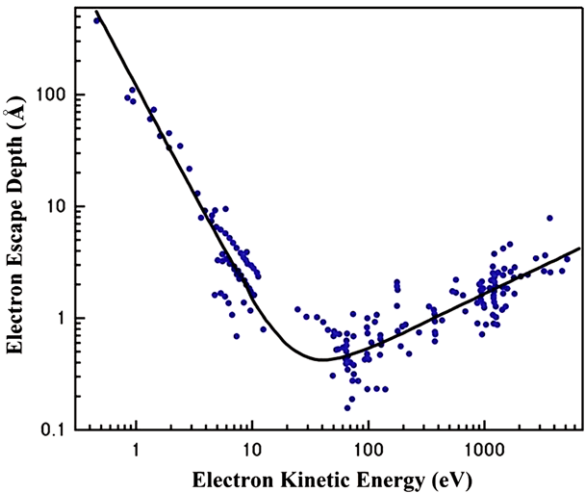

Fig. 2.4 Universal curve of photoelectron mean free path as a function of photoelectron energy [19]

mode and even worse is that it usually has a large spot size and a fast aging effect of sample because of the flowing helium. For the regular synchrotron radiation light source, its flux and bandwidth are irreconcilable, and by this reason, in the actual ARPES applications, it is difficult to achieve a high-resolution within meV. The regular working energy resolution of today's most advanced synchrotron radiation light source is generally around 10 meV. Nonetheless, the usual physical properties of materials are determined by valence band electrons with an energy scale a few k_BT (k_B is Boltzman constant, T is temperature) near the Fermi level. At low temperatures, such as $T = 10$ K, k_BT to energy is less than 1 meV, so it's necessary to develop experimental instruments with energy resolution at the order of 1 meV. For many superconducting materials, in order to study the most important parameter-energy gap, the energy resolution should be better than 1 meV.

Another problem of photoelectron spectroscopy techniques is the extreme sensitivity of surface because the escape depth of photoelectrons is very short for regular photons which is usually between 20∼100 eV (Fig. 2.4) [19]. For photons with energy 20∼50 eV, the escape depth of photoelectrons is merely 5∼10 Å which means that only electrons in the top layer of materials could escape into vacuum. For advanced materials, the most properties we concerned is bulk parameters rather than that from surface effect. One of the methods to increase the probe depth is using photons with higher energy. For example, the escape depth is ∼20 Å for a photon energy of 1000 eV. However, high energy photons will give a bad momentum resolution of 0.05 $Å^{-1}$, taking 1000 eV for example [20].

As shown in Fig. 2.4, another method to increase the probe depth is to reduce the photon energy, and moreover, it's easy to get good momentum resolution (Eq. 2.4). Based on these advantages, it is natural to consider using and ultraviolet laser as a light source in photoemission experiments and many attempts have been done with this idea. However, only series of crucial conditions have to be met before the laser can be used in high-resolution photoemission experiments,

1. High photon energy. The energy of photoelectrons should be high enough to overcome the work function of materials which is usually 4∼5 eV. The photon energy should be higher than 5 eV.
2. High photon flux. The flux of laser should be enough to produce reasonable quantity of electrons which are counted by electron energy analyzer.
3. Narrow bandwidth. The bandwidth determines the energy resolution of light source.
4. Continuous wave or quasi continuous wave. The pulse length of regular laser is very short and the number of photons in each pulse is high, and it will bring enhanced space charge effect to deteriorate the energy resolution.
5. Compatible electron energy analyzer. To take the advantage of narrow bandwidth laser, the electron energy analyzer should work at low energy with high resolution.

Because of these limitations, the high resolution laser-based ARPES is only developed recently by the application of quasi-continuous wave violet laser which significantly reduces the space charging effect. Moreover, the newly discovered nonlinear optical crystal $KBe_2BO_3F_2$(KBBF) [1, 21–23] brought the possibility of frequency multiplication in ultra-violet waveband, the application of which made significant progress in the photoemission technique. With the application of KBBF, Shin group successfully obtained quasi-continuous wave laser with photon energy 6.994 eV and combined it with photoemission technique, achieving an energy resolution better than 1 meV for the first time in the world [24, 25]. The total energy resolution they got is 0.36 meV which is a combination of the bandwidth of laser 0.26 meV and the resolution of electron energy analyzer 0.25 meV. However, the photoemission system of this group had no momentum resolution before 2006, and this greatly reduced the power of photoemission technique. Individually, Dessau group developed an ARPES system with total energy resolution 8 meV by the application of a violet laser with photon energy 6.05 eV and bandwidth 4.7 meV [26, 27], and they could only probe small momentum region in the Brillouin zone because of such low photon energy.

With the corporation of our group, Chuangtian Chen group and Zuyan Xu group, we developed the first VUV-based ARPES system with energy resolution better than 1 meV in 2006 [2]. The Chen group provided us the second harmonic KBBF crystal, and Xu group cooperated with us to design the laser system and completed the optics setup, as shown in Fig. 2.5. The following section will mainly focus on the design and test of the system [2].

2.3.1 VUV Laser Light Source

It's a simple and direct way to obtain the VUV laser by using the second harmonic light of nonlinear optical crystal. Applicable nonlinear optical crystal should have large nonlinear optical coefficient, absorption edge less than 200 nm and property index of refraction (usually between 0.07 and 0.10).

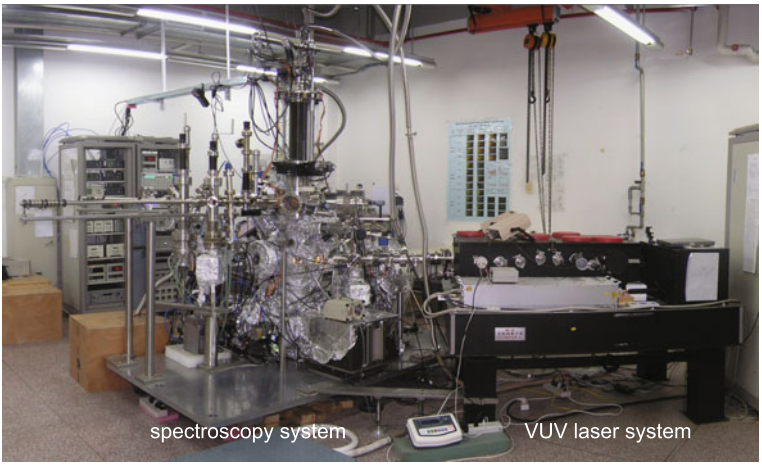

Fig. 2.5 VUV laser-based ARPES system

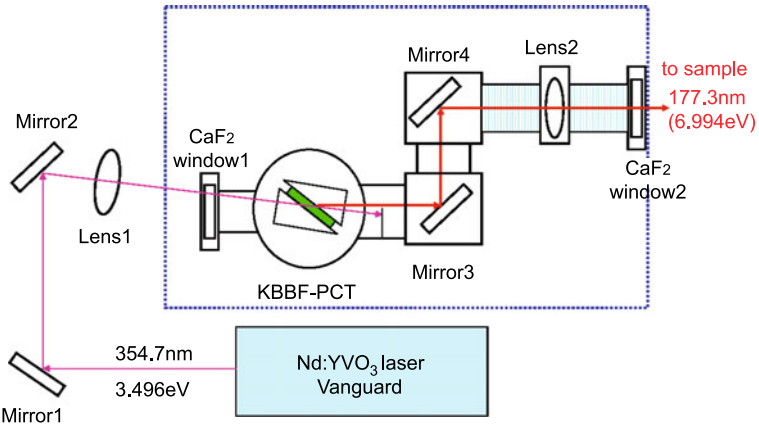

Fig. 2.6 A schematic layout of our VUV laser optical system [2]

Nonlinear optical crystal we use is the $KBe_2BO_3F_2$ (KBBF) grew by Chen group. The crystal has good nonlinear optical properties-good transmission and high index of refraction. Moreover, comparing to other nonlinear optical crystal, KBBF has a wider reception angle; the reception angle is 0.290 (mrad/cm), taking the second harmonic process of generating 177 nm photons from 355 nm laser for example. Because of the layer structure of KBBF and the difficulty of growing large size crystals, it's hard to reach the phase-matching angle by simple cutting. In actual using, a prism coupling technique was developed to solve this problem. The 177.3 nm VUV laser used in our ARPES system is generated by the second harmonic processing of the original 355 nm laser through a KBBF-PCT device; the related optical system is schematically shown in Fig. 2.6. The pump laser is a commercial laser (Vanguard,

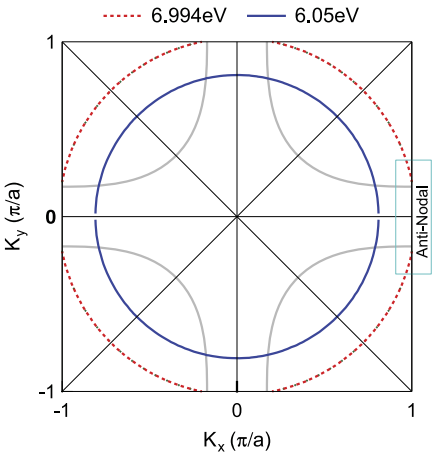

Fig. 2.7 The momentum region probed by 6.994 eV photons and 6.05 eV photons

Spectra Physics) with wavelength 354.7 nm, pulse length 10 ps, and total power 4 W. The VUV laser entering into the ARPES chamber is the second harmonic component with wavelength 177.3 nm.

The total optical system should be installed in a vacuum chamber with pressure better than 10^{-5} Torr, for the air has a large absorption of photons with energy higher than 6.5 eV. Actually in our system, the system is put in a sealed chamber with flowing pure nitrogen which has a low absorption rate of 177 nm photons. Comparing to the 6.05 eV laser with a bandwidth 4.7 meV used in the Dessau group [26, 27], our 6.994 eV laser has ultra-high resolution with bandwidth 0.26 meV. Moreover, the higher photon energy we use could probe larger momentum region in the Brillouin zone. For regular cuprate materials studied by ARPES, the typical work function is around 4.3 eV, and the maximum momentum could be probed by 6.994 eV photons is $1.02/a$ but $0.81/a$ for 6.05 eV photons; here a is the length of the Cu-O-Cu bond. As shown in Fig. 2.7, 6.994 eV could reach the antinodal region the electrons of which plays an important role in cuprate materials, while it's impossible for 6.05 eV photons.

Comparing to synchrotron light source most widely used in ARPES experiments, VUV laser has lots of advantages. The cost of the VUV laser is much lower and the size is much smaller, and more importantly, the VUV laser has ultra-high energy resolution without expending photon flux. Moreover, the bulk sensitivity is enhanced by using low energy photons. As shown in Fig. 2.4, for photon energy 6.994 eV, the energy of excited electrons is around 6∼6.994 eV with escape depth around 30 Å but this value is only several Å for regular used photon energy 20∼30 eV on synchrotron. By Eq. 2.9, for lower photon energies used, higher momentum resolution could be reached.

However, there are also some shortcomings for VUV laser in ARPES experiments. First, lower photon energy of the VUV laser only probes electronic states near Fermi level, but for a synchrotron light source and gas discharge lamp, not only valence band but also the inner-shell electronic structure could be probed. Second, the involved matrix element effect in the ARPES experiment which is as a function

Table 2.1 Comparison of the performance with different light source-VUV laser, synchrotron light source and gas discharge lamp

Light source	VUV laser	The best synchrotron	Gas discharge lamp
Bulk sensitivity	30∼100 Å	5∼20 Å	5 Å
Energy resolution (meV)	0.26	5∼20	1.2
Momentum resolution	best		
Photon flux (/s)	2×10^{15}	$10^{12}10^{13}$	10^{12}
Spot size	∼0.2 mm	∼0.2 mm	1∼3 mm
Polarization	tunable	tunable	no or part
Photon energy (eV)	5∼7	tunable 5∼1000	21.2He I
Momentum region	about 1 BZ	many BZs	many BZs
Sample quality	high	rigorous	rigorous
Cost	high	very high	high

of the photon energy and polarization couldn't be controlled by VUV laser which has only single photon energy, but the photon energy of the synchrotron light source is tunable. Last, small momentum region in the Brillouin zone could be reached by the low photon energy of the VUV laser; For a synchrotron light source, with higher photon energy, it could probe several Brillouin zones at the same time and it's easy to map the Fermi surface of materials. Table 2.1 shows the comparison of the performance of different light sources in ARPES experiments.

To compensate the disadvantage of a VUV laser, a gas discharge lamp (the product of Gammadata) is equipped on our ARPES system. With available photon energy 21.2 eV and 40.8 eV from the discharge lamp, the function of the ARPES system is much more expanded. Moreover, a tunable VUV laser system will be developed, and the effect of matrix element will be improved.

2.3.2 Spectroscopy System

ARPES basically consists of four major components, including light source, electron energy analyzer, sample manipulator and ultra high vacuum (UHV) system. This section will make an introduction to these components on spectroscopy system individually.

(1) **UHV system**

The surface of the sample is very sensitive for ARPES experiments, and it's necessary to keep the surface clean for a reasonable long time. By simple estimation, in the vacuum with pressure 10^{-6} Torr, a clean surface will be covered by one layer of atoms in one second. Generally, regular ARPES experiments usually last for one or two days, so the pressure of the analysis chamber should be kept below 10^{-10} Torr.

To obtain UHV below 10^{-10} Torr, the chamber should be made by UHV compatible material. Except special demand, the chambers usually are made by stainless steel, and electro-polished method is applied to the inner surface of the chambers to reduce the gas adsorption. The leak rate of the chamber should be lower than 10^{-10} Torr.

Bunch kinds of vacuum pump are used to achieved UHV,

1. Dry vacuum pumps, which are used to obtain rough vacuum (10^{-2} Torr) as a pre-pump of turbomolecular pump. It has advantages of oil-free and high pumping speed.
2. Mini-TASK Turbo Pumping System, a small and compact, easy-to-use integrated dry vacuum system featuring the Varian Turbo-V 81 MacroTorr pump with improved vacuum performance. The base pressure could be better than 10^{-8} Torr.
3. Turbomolecular Pump. The base pressure of this kind of pump is better than 10^{-10} Torr. For chambers with different size and load, turbo pumps with different pumping speed should be selected. The pumping speed of turbo pumps we use on main analysis chamber and the monochromator of helium discharge lamp are 500 l/s, two turbo pumps with pumping speed 300 l/s are used on the load lock system, and two pumps with pumping speed 70 l/s are used as differential pumps on helium discharge lamp.
4. Cryopump. A cryopump is a vacuum pump that traps gases and vapours by condensing them on a cold surface, and it is used on the main analysis chamber and compatible with UHV.
5. Titanium sublimation pump (TSP). It consists of a titanium filament, and the titanium is sublimated to coat the chamber wall. Since clean titanium is very reactive, components of the residual gas in the chamber which collide with the chamber wall are likely to react and to form a stable, solid product. The TSP is used to achieve UHV in main analysis chamber.
6. Ion pump. It's a type of vacuum pump capable of reaching up to 10^{-11} Torr under ideal conditions and commonly used in ultra high vacuum (UHV) systems.
7. Getters. It's made by high porosity St172 sintered material, and it has high pumping speed for all active gases especially the H_2. It's usually used to get better UHV.

Vacuum measurement tools are essential in the vacuum chamber system. Three kinds of vacuum gauges are used on our system, including Granville-Philips 360 iron gauge, Granville-Philips 370 iron gauge and convection gauge. The style of 360 and 370 are used to measure high vacuum better than 10^{-4} Torr, but 370 is more accurate after calibration. The convection gauges are used to measure rough vacuum from 1 atm to 10^{-4} Torr.

Baking up the chamber is necessary to obtain UHV. The purpose of baking is to get rid of the gases adsorbed on the inner wall of the chamber. Usually, the baking temperature used is 150 °C, but some special temperature is used for special parts. Before the baking, the pressure in the chamber should be better than 10^{-7} Torr which could be achieved by pumping with the pre-pump and turbo pump. Usually, the baking lasts for 3$\sim$7 days depending on condition of the chamber. It's better to

turn on the cryopump and ion pump to pump out the dirty gas before turning off the baking, and at the same time, degas all the filaments in the chamber.

(2) **Mu metal chamber**[1]

During the photoemission process, the emission angle of photoelectrons carries the momentum information of electrons in materials. To make sure the path of photoelectrons in the vacuum chamber isn't disturbed by any field, it's necessary to minimize the remanent magnetic field around the path of photoelectrons. For laser-based ARPES experiments, the energy of photoelectrons is low which is much sensitive to the remanent magnetic field in the chamber, so it's much rigorous to screen the geomagnetic field and the other magnetic field. Actually, to minimize the magnitude of the magnetic field, our analysis chamber was made by mu-metal. In addition, a sheet of magnetic shielding made by mu-metal was inlaid in the chamber. After installation, a process of demagnetization was made to remove the remanent magnetic flux. By these detailed design and demagnetization, the remanent magnetic field around the sample position achieved a very low level with total 0.8 mG and the components of three directions are 0.1 mG, 0.5 mG and 0.6 mG.

(3) **Electron energy analyzer**

Electron energy analyzer is one of the core components on ARPES system. Most of nowadays ARPES systems are using a hemispherical energy analyzer which consists of multi-stage electrical lens and a hemispherical deflection analyzer and is made by two concentric hemispheres with radius R_1 and R_2. A constant voltage V is applied between the two hemispheres when it works, and only electrons within energy window $E_p/10$ around $E_p = e\Delta V/(R_1/R_2 - R_2/R_1)$ could go through the hemispherical deflection analyzer and be counted by a CCD detector. The energy resolution could be defined as

$$\Delta E_\alpha = E_p\left(\frac{w}{R_0} + \frac{\alpha^2}{4}\right) \tag{2.9}$$

with $R_0 = \frac{R_1+R_2}{2}$, and w is the width of entrance slit and α is the acceptant angle.

The energy analyzer we used is a R4000 (product of SCIENTA) hemispherical energy analyzer of which the energy resolution could be better than 1 meV. For example, when slit size is 0.1 mm and pass energy E_p is 1 eV, the resolution of the analyzer is 0.25 meV. Combined with VUV laser (bandwidth 0.26 meV), the total energy resolution of our ARPES system could be better than 1 meV. Another unique feature of the R4000 energy analyzer is its two-dimensional measurement capability, which makes it possible to simultaneously measure a wide range of angles of photoelectrons. However, it's a challenge for probing such low energy photoelectrons stimulated by the VUV laser. Much effort was made to optimize the lens table of the analyzer, and ultimately the electron energy analyzer could work with wide

[1]Mu-metal is a nickel-iron alloy (approximately 75 % nickel, 15 % iron, plus copper and molybdenum) that has very high magnetic permeability.

angular mode at such low energy. At last, three different angular mode including 30°, 14° and 7° with three sets of different lens table for three different spot sizes (2.0 mm, 0.8 mm and 0.1 mm) are selectable in experiments.

(4) **Sample transfer system**

There is a preparing chamber upon the mu-metal analysis chamber which could be isolated from the analysis chamber by a UHV hand gate valve. This kind of design brings the convenience of the maintenance of cryostat. By closing the hand gate valve, the analysis chamber could be kept in UHV and just the top preparing chamber needs to be vented when we pull out the cryostat. In the preparing chamber, a wobble stick, an argon sputtering gun and a LEED are equipped to cleave, clean and characterize the sample. Moreover, a residual gas analyzer (RGA) is equipped to analyze the components of gases in the chamber, and it's convenient to do leak tests by spraying helium around the chamber. To transfer the sample from 1 atm air to UHV preparing chamber without venting and baking the chamber, a load-lock system with two stages is directly connected to the preparing chamber. After venting the first stage of load-lock with pure nitrogen, one can transfer samples into the first stage chamber and pump it until the pressure below $10^{-7}\sim10^{-8}$ Torr; Then open the valve between the first and second stage and transfer the samples to second stage chamber. Usually, the pressure in the second stage chamber is $10^{-10}\sim10^{-11}$ Torr, and it's safe to transfer the sample to the preparing chamber directly without destroying the vacuum.

(5) **Cryostat**

The sample manipulator is a product of VG (VG, Centiax Translator) to control the translational motion along X, Y, Z direction and the polar rotation (ϕ). The cryostat we ordered has the rotational dimensions along the other two axes, the tilt (θ) and azimuthal (ω), as shown in Fig. 2.8. Then the orientation and position of sample on the cryostat could be fully controlled, and all the motions are controlled by stepper motors. Moreover, we have developed a Labview program to control the motor on a computer. The error and repeatability of rotations is 0.005° and the error of motion along X, Y and Z axes is 0.001 mm, 0.001 mm and 0.01 mm. The sample on the cryostat is cooled by flowing liquid helium and the lowest temperature is lower than 12 K. At the same time, the temperature of sample could be controlled by a heater mounted on the cold tip of cryostat. The temperature of sample could be varied between 12 K and 450 K by an advance PID temperature controller and could be stabilized within 0.1 K. The temperature is measured by a standard silicon dioxides (LakeShore, DT-471), and the error is within 1 K. To minimize the variation of sample position by thermal expansion and contraction effect, the sample stage is fixed on a tube made by stainless steel, and connected to the cold tip by a flexible copper braid. Moreover, a copper shielding is equipped to block the radiation from outside environment. To isolate the magnetic field, only non-magnetic materials and parts are used to manufacture the cryostat.

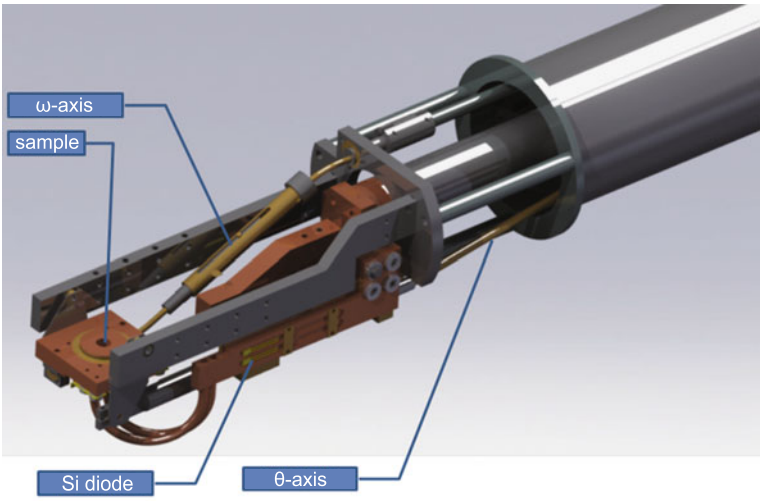

Fig. 2.8 Model of the six-axes cryostat

2.3.3 Performance of the System [2]

(1) **Energy resolution**

With a general method, we measured the width of Fermi edge of a clean polycrystal gold to extract the energy resolution of this ARPES system. Figure 2.9 shows the spectra measured at 9.22 K with energy analyzer settings $E_p = 2$ eV and slit $= 0.1$ mm. By fitting the curve with Fermi-Dirac distribution function, the width of Fermi edge at hight from 12 % to 88 % is 3.211 meV. The calculated energy resolution of the system is 0.56 meV by taking off the temperature broadening which is about 3.162 meV. The total energy resolution came from three components include the bandwidth of the VUV laser (0.26 meV), resolution of the electron energy analyzer (for $E_p = 2$ eV and slit $= 0.1$ meV, resolution is 0.5 meV) and space charging effect which is determined by spot size and photon flux. In this case, the measured energy resolution is quite consistent with the nominal resolution given by convolution results of the VUV laser bandwidth and energy resolution of the analyzer.

It is noteworthy that during the test we didn't use a better resolution of electron energy analyzer by setting $E_p = 1$ eV which would give a total energy resolution 0.36 meV, because the temperature broadening is comparable with the measured width of Fermi edge which could bring great uncertainty when taking off the temperature broadening. Anyway, Kiss *et al.* measured gold at temperature 2.9 K and get a good resolution 0.36 meV [24]. We didn't measure the highest resolution of our system. However, the laser we used is similar to the one Kiss *et al.* reported in the paper [24]. So, it's reasonable to believe that the best resolution of our ARPES system is ~0.36 meV.

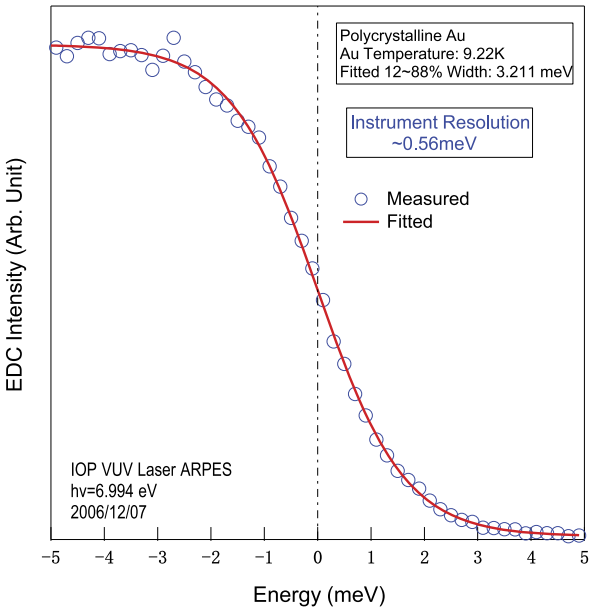

Fig. 2.9 Energy resolution test of VUV laser-based ARPES. Spectra of a polycrystal gold measured at 9.22 K. Reprinted with permission from [2], copyright 2008, American Institute of Physics

(2) **Photon flux test**

The power of the outgoing beam from KBBF-PCT device was measured by a power meter (LP-3A, Physcience Opto-electronics Co., Ltd., Beijing) which had been calibrated by 532 nm green laser in National Institute of Metrology. The out put power of 177 nm beam from KBBF-PCT (0.8 mm) pumped by 355 nm laser with power 2 W is 1.68 mW, and by increasing the pump power or thickness of KBBF, the output power would be enhanced. Under the assumption that the factor of the power meter by calibration at 532 nm and 177 nm were the same, the output photon flux should be 1.5×10^{15} photons/s which was two to three orders higher than the third generation synchrotron radiation light source, and at the same time, the bandwidth was one order narrower than the synchrotron radiation light source. For regular synchrotron radiation light source, the energy resolution is 10∼15 meV, although for some individual cases the resolution of the demonstration could achieve 4 meV.[2]

As the fluctuation of temperature in the room within 2 °C, the output power of the laser could be stabilized with an error no more than 5 %. Such high stability is the ideal condition for ARPES experiments. Because of thermal accumulation and radiation, a local area (∼100 μm) of CaF_2 or KBBF would be damaged after

[2]Such high resolution realized at synchrotrons with low-energy storage rings in recent years. For example, Hiroshima Synchrotron Radiation Research Center in Japan, http://www.hsrc.hiroshimau.ac.jp with related literature [28] and Borisenko group in Dresden of Germany, http://www.ifw-dresden.de/institutes/iff/research/SC/arpes.

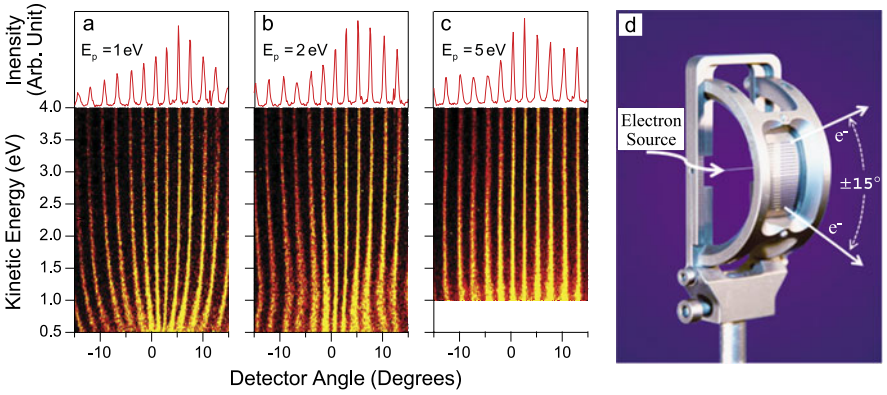

Fig. 2.10 Angular mode test results of R4000 electron energy analyzer [2]. (**a**), (**b**) and (**c**) are the test results of pass energy 1 eV, 2 eV and 5 eV, individually. (**d**) is the slit-wire device used in the test. (**a**), (**b**) and (**c**), Reprinted with permission from [2], copyright 2008, American Institute of Physics

working for tens of hours. Usually, the laser incident position on KBBF-PCT device requires regular adjustment to gain reasonable out power.

(3) **Angular mode test**

The angular mode test was carried on by using a specially designed slit-wire device (Scienta), as shown in Fig. 2.10(d). By using a electron gun hit a thin wire in the center of the device to simulate the signal from samples, and two adjacent slits represent a specular emission angle (2.5° in our test). Figure 2.10(a), (b) and (c) show the test results of 30° angular mode with pass energy $E_P = 1$ eV, 2 eV and 5 eV separately, and during the test the spot size is set to 0.1 mm. From Fig. 2.10, we can see that the electron energy analyzer works quite well at energy at least above 0.5 eV which is quite suitable for our ARPES system equipped with a 6.994 eV laser. For the 6.994 eV laser, the maximum energy of emission photoelectrons is about 2.694 eV. From the test results, we could estimate that the angular resolution is 0.3° for 14° angular mode and 0.8° for 30° angular mode when the spot size is 0.8 mm. It is noteworthy that the angular resolution is sensitive to the spot size that the angular resolution is better for smaller spot size. The slit-wire device shown in Fig. 2.10(d) doesn't work for testing the angular resolution with laser spot size of 0.1 mm, so we couldn't get the value of angular resolution when slit is 0.1 mm but it's far better than 0.8° which is the test result of the 30° angular mode when slit size is 0.8 mm.

Usually, what's our concern is the momentum resolution in resolving the fine band structure in material. Using Eq. 2.4 to translate the angular resolution to momentum resolution, we can find that the momentum resolution could be improved by using low photon energy. For example, the momentum resolution of photon energy 6.994 eV is 0.4 times smaller than of the helium lamp with photon energy 21.2 eV.

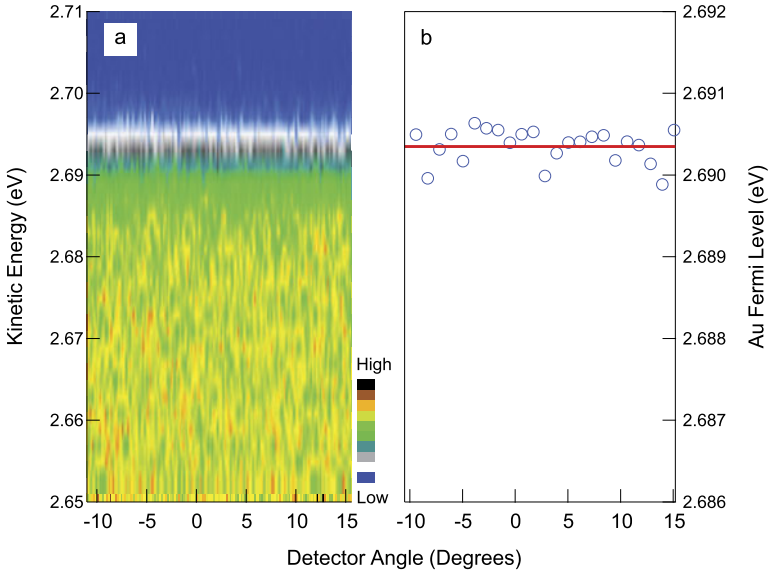

Fig. 2.11 The distribution of Fermi edge measuring a gold with angular mode by VUV laser. Reprinted with permission from [2], copyright 2008, American Institute of Physics

Another important aspect we usually concern is that the uniformity of energy at different receipt angles. For some older styles of energy analyzer or some analyzers working at low energy, the measured Fermi edges at different angles were not the same, and it would bring some difficulties and annoyance to analyze the data. We have measured the Fermi edge of gold with angular mode at low temperature to check if it was a problem for our electron energy analyzer or low energy laser light source. Figure 2.11(a) shows the spectra of Fermi edge measured with 30° angular mode, and Fig. 2.11(b) shows the fitted position of Fermi edge as a function of receipt angle from which we can see that the analyzer works perfectly with the 6.994 eV laser that the distribution of Fermi edge is within 0.3 meV.

(4) **Bulk sensitivity test**

The bulk sensitivity is expected to be enhanced by using a VUV laser when probing the electronic structure in solid materials by ARPES. From the universal curve (Fig. 2.4) of electron escape depth as a function of electron energy, the escape depth of photoelectrons by a 6.994 eV laser is about 30 Å or even 100 Å. Noting that the universal curve was by measuring the mean free path in simple metals, we are not sure if it's suitable for complex oxides.

To overcome the difficulty of measuring the electron escape depth in oxides, we took the comparison of measuring results on Bi2212 single crystal under different conditions to check whether the bulk sensitivity is enhanced or not. First, we cleaved a optimally doped Bi2212 ($T_c = 90$ K) in UHV at 17 K, and the measured $(0, 0)$–(π, π) dispersion is shown in Fig. 2.12(a). Second, we pulled the sample and

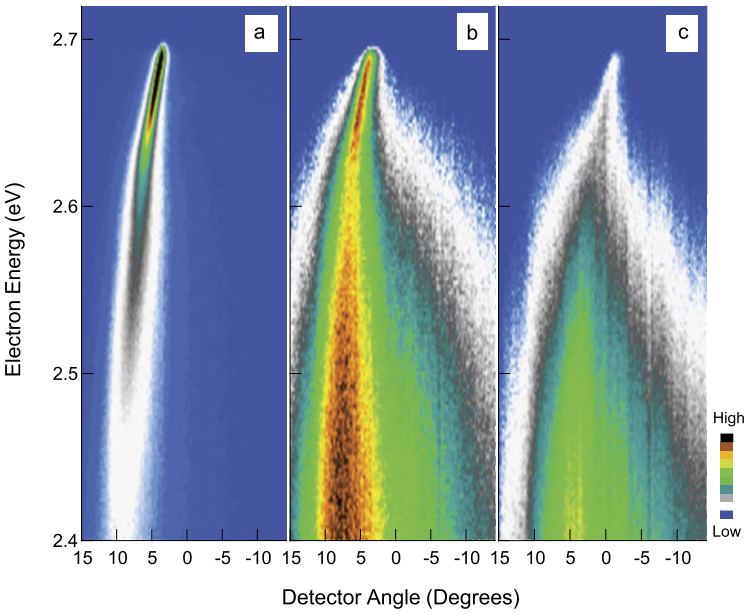

Fig. 2.12 The bulk sensitivity test of 6.994 eV laser-based ARPES system on an optimally doped Bi2212 ($T_c = 91$ K). (**a**) The dispersion right after cleaving. (**b**) The dispersion after keeping in pure nitrogen for 1 hour. (**c**) The dispersion after keeping in air for 1 hour. Reprinted with permission from [2], copyright 2008, American Institute of Physics

transferred it into the first stage of the load-lock system, and then vented the chamber with pure nitrogen; Fig. 2.12(b) shows the same measuring result after keeping the sample in pure nitrogen for one hour. Last, we pulled out the sample out of the chamber and kept it the air for one hour, and Fig. 2.12(c) is the measuring result after reloading the sample into analysis chamber. All the measurements were taken at low temperature. It was easy to get dirty on the surface of the sample when the sample exposed in nitrogen or air, and the photoelectron signal would become weak and come with much more secondary electrons. However, it's beyond belief that the main feature of the dispersion was still there, as we can see in Fig. 2.12 which couldn't happen when using 20∼50 eV photons.

Enhanced bulk sensitivity doesn't only extend the life of the sample, but also reduce the requirement of sample surface preparation. This will bring the possibility of ARPES measurement on some uncleavable sample by heating or ion sputtering.

(5) **Space charging effect test**

The space charging effect in photoemission experiments may be a problem in laser-based ARPES for its high photon flux and pulse characteristic. We measured the shift of the Fermi level and width of the Fermi edge of a gold at 9.2 K with different photon flux to test the space charging effect on 6.994 eV laser-based ARPES system.

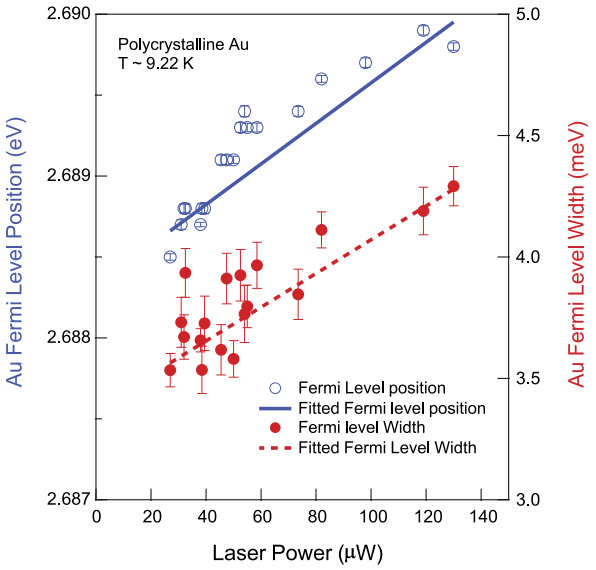

Fig. 2.13 The space charging effect test of the 6.994 eV laser-based ARPES system. Reprinted with permission from [2], copyright 2008, American Institute of Physics

Figure 2.13 shows the position of Fermi level and width of Fermi edge as a function of photon flux. The shift of the Fermi level is about 1.5 meV when tuning the power of the laser to 130 μW, and the broadening of Fermi edge is about 2.5 meV. It's clear that the spacing charging effect is still there on the laser-based ARPES system, but it's much weaker than the observation with a synchrotron light source. Many aspects are responsible for such a low space charging effect. First, the quasi-continues characteristic of our laser with repetition frequency 80∼100 MHZ could greatly reduce the space charging effect. Second, the spacing charging effect has a direct connection with the sum of outgoing electrons; Comparing to synchrotron light source, the total number of photoelectrons is much less because the VUV laser would reduce the energy window of photoelectrons and bring much less secondary electrons. Last, because the balance between space charging effect and mirror charge effect, the total effect depends on the pulse length; In the simulation by X.J. Zhou *et al.* [29], the space charging effect and mirror charge effect will cancel each other when the pulse length is 1∼10 ps which is just the value of our VUV laser.

(6) **Typical measurment on Bi2212**

Because of its easy cleaving and popularly studied, a piece of high-temperature superconductor Bi2212 sample was selected as a standard sample to test the performance of the VUV laser-based ARPES system. Figure 2.14(a) shows the original spectra along nodal $\Gamma(0,0) - Y(\pi,\pi)$ cut with total energy resolution 1 meV, and the well-known 70 meV kink structure was well reproduced by laser ARPES. The sharp energy distribution curve (EDC) at Fermi momentum and the momentum distribution curve (MDC) shown in Fig. 2.14(b) and Fig. 2.14(c) individually demonstrate the quality of the data. The width of the nodal EDC we got in optimally doped Bi2212 is 12 meV and this value is 9 meV in a underdoped sample ($T_c = 75$ K)

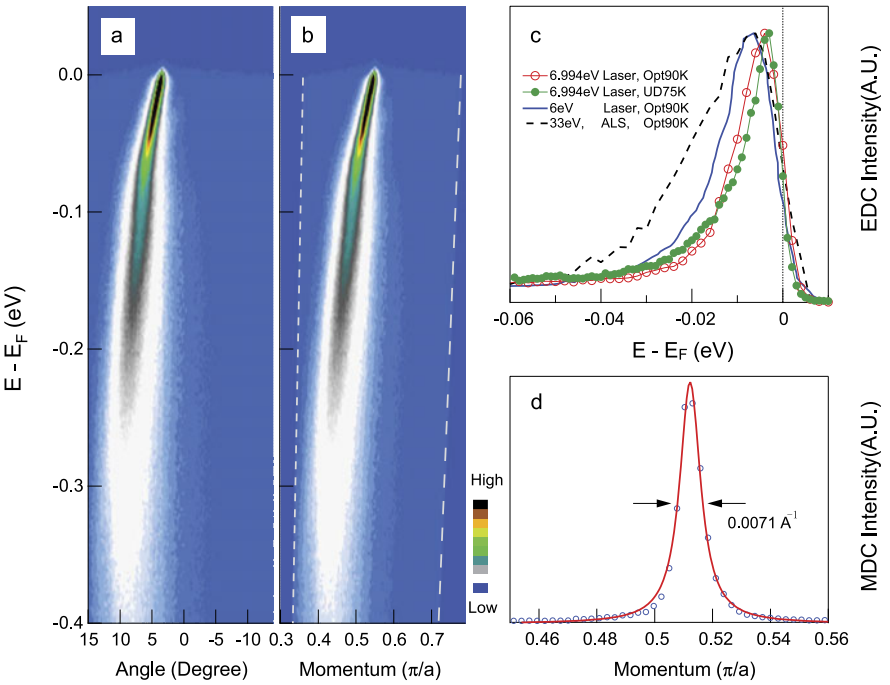

Fig. 2.14 Typical measurement on a Bi2212 samples by 6.994 eV laser-based ARPES. Reprinted with permission from [2], copyright 2008, American Institute of Physics

which is much more improved than the value 25 meV got on synchrotron light source and also sharper than the value 14 meV but by 6 eV laser. Much improved quality of the spectra was attributed to the ultra high energy resolution, momentum resolution and low temperature of the sample. Also, the value of MDC width 0.0071 Å^{-1} is much sharper than that got on synchrotron light source.

We also noted that the using of low energy photons brings the change of the way of processing data. When translating the emission angle θ into electron momentum parallel $k_{\parallel}(\text{Å}^{-1})$ to sample surface, Eq. 2.3 is used and the uncertainty of the sample work function is usually negligible for high photon energy 20∼50 eV. But the situation is changed for lower energy photons like 6.994 eV. Figure 2.14(b) shows the dispersion image after apply the correction of binding energy, from which we can find that the momentum edge was not vertical anymore. This kind of correction is more significant for lower energy photons like 6 eV.

2.4 The Development of Spin-Resolved ARPES, Time-of-Flight ARPES and Tunable Laser ARPES Systems

With the experience and success of developing first VUV laser-based ARPES, we developed a spin-resolved ARPES system equipped with the VUV laser which

would improve the energy resolution and detection efficiency of spin resolved experiments. Moreover, based on the new style of electron energy analyzer (ARTOF10K of Scienta), a new ARPES system was developed to improve the momentum resolution and efficiency of data acquisition. In addition, we will make an upgrade on the original VUV ARPES system with a tunable VUV laser which will improve the matrix element effect induced by the photon energy in ARPES experiments.

2.4.1 The Development of Spin-Resolved ARPES

Regular ARPES systems only probe the electronic structure with only energy and momentum, as shown in Fig. 2.3. According to quantum mechanics, the full electronic state in materials should contain three parameters, including energy, momentum and spin. So, it's important to develop spin resolved equipments in the study of solid materials especially spin electronic materials. To realize the detection of electronic spin, the most popular detector used is the Mott spin detector.

Because of the spin-orbital coupling, the distribution of scattering electrons by heavy nucleus is anisotropic in different direction which is called Mott scattering, and the design of Mott spin detector is based on such an effect [30–39]. For electron beam with polarization **P**, the scattering cross-section is

$$\sigma(\theta) = I(\theta)\left[1 + S(\theta)\mathbf{P}\cdot\mathbf{n}\right] \tag{2.10}$$

with scattering angle θ, scattering intensity $I(\theta)$, unit vector perpendicular to the scattering plane **n** and Sherman function $S(\theta)$ which is determined by the atomic number Z, scattering angle θ and the energy of scattering electrons. The specular feature of Mott scattering is that the asymmetrical scattering attributes to the electrons with polarization perpendicular to the scattering cross-section. The electronic polarization could be detected by analyzing the asymmetrical scattering intensity, and this kind of spin detecting method has been used in the Mott detector.

The actual process of spin detection is shown in Fig. 2.15(a), in which the detector is combined with a hemispherical electron energy detector and a Mott spin detector. The schematic of a Mott detector is shown in Fig. 2.15(b) [40]. The Mott scattering happens when electrons eject into the surface of a heavy metal, and the distribution of scattering electrons is different for electrons with different spins. By comparing the counts of two electron counters, the polarization perpendicular to the ejecting election could be calculated by Eq. 2.11, in which the I_L and I_R are the count of the two electron counters.

$$P = \frac{1}{S}\frac{I_R - I_L}{I_R + I_L} \tag{2.11}$$

For actual Mott detector, the efficiency of the two electron counters usually have several percents of difference. To cancel the asymmetrical efficiency of the two electron counters, usually two electron beams with opposite polarization are used to

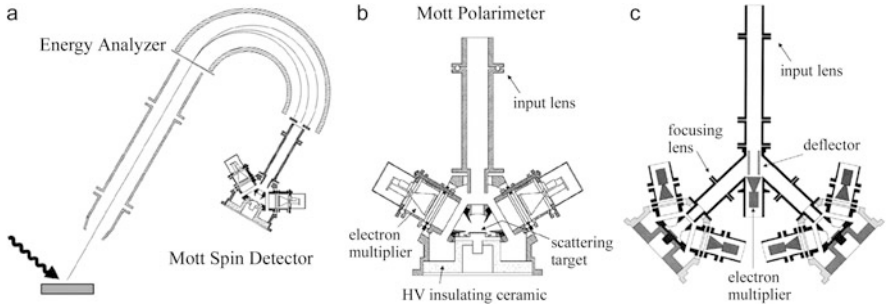

Fig. 2.15 The schematic of spin detection. (**a**) The process of detecting spin, energy and momentum state in material. (**b**) The schematic of Mott spin detector. (**c**) The concept schematic of full polarization detector. Here only the electron multipliers pair in the paper plane are shown. Reprinted with permission from [40], copyright 2002, American Institute of Physics

calibrate the detector. So the calibrated polarization is

$$P = \frac{1}{S}\frac{1-\alpha}{1+\alpha} \tag{2.12}$$

in which α is $\sqrt{I'_L \cdot I_R / I_L \cdot I'_R}$, and the I'_L and I'_R are the counts of the two electron counters for incident electron beam with polarization $-\mathbf{P}$.

A concept schematic for probing the full polarization (projection to X, Y and Z axes) of electrons was proposed by Huang *et al.* in 2002 [40], as shown in Fig. 2.15(c). The incident electron beam is split by an electrostatic deflector and enters into two spin detector with a direction at 45° to the ejecting beam. Moreover, regular ARPES experiments could be proceeded at the same time by deflecting electrons into a MCP detector. Each isolated spin detector could probe two sets of orthogonal polarization, and the full polarization with three components (P_x, P_y and P_z) could be derived by a coordinate transformation. A self consistent check could be done by comparing the components of polarization perpendicular to paper plane from the two spin detector pairs.

With cooperation with Scienta, based on a R4000 hemisphere electron energy analyzer and a Mott detectors designed by Rice University, we developed a new spin polarization ARPES system as shown in Fig. 2.15(c). Figure 2.16(a) shows the three-dimensional model of a R4000 electron energy analyzer and Mott spin detectors. A little different from Fig. 2.15(c), the two Mott detector pairs are perpendicular to the incident electron beam. The horizontal one probes the polarization P_y, P_z along Y, Z directions, and the vertical one probes the polarization P_x, P_y along X, Y directions. Here the P_y detected by the two detector pairs individually could be used to do the self-consistent check. Moreover, the regular angular resolved mode is kept but shrinking the hole of regular angular detection, and the maximum detecting angle is ±15° which is a little smaller than a regular R4000 analyzer. Figure 2.16(b)[3]

[3]Technical document from website VG Scienta.

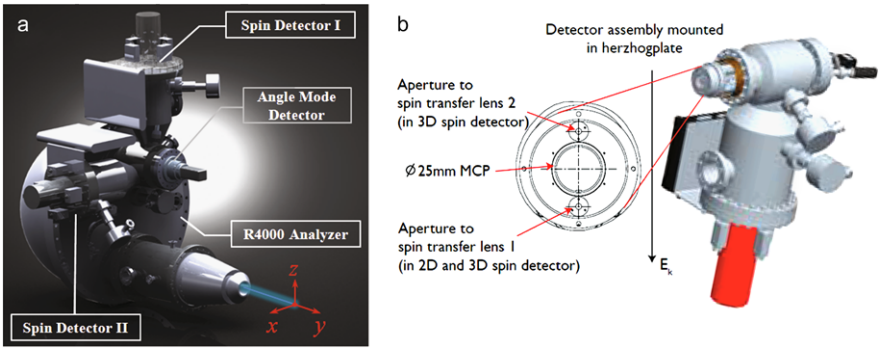

Fig. 2.16 (**a**) The 3D model of the combination of R4000 analyzer and Mott detectors. (**b**) The schematic of the apertures for spin and regular angular detection

shows the schematic of the spin detectors, in which there are two tiny apertures for the two spin detectors and a 25 mm aperture for regular ARPES measurement.

The cross-section of Mott scattering is rather low, usually between 2×10^{-5} and 1.6×10^{-4}. With such a low scattering efficiency, the counts of Mott spin detectors are usually only 1/10000 or 1/100000 of regular ARPES. To get reasonable counts, people usually reduce the energy resolution (usually 100 meV) and integrate the spectra over a wide angle (angle integrated photoemission spectroscopy) in regular spin resolved experiments with Mott spin detectors. Another simple way to get reasonable counts without giving up the energy and angular resolution is increasing the flux of incident photons, but it's impossible for synchrotron light source and gas discharge lamp for the reason that increasing the photon flux will broaden the bandwidth of photons for synchrotron light source and the photon flux of gas discharge lamp is not tunable.

Application of the VUV laser with high photon flux is one of the promising approaches to overcome the limitation of energy resolution in spin resolved experiments. By upgrading the second harmonic generation system and improving KBBF crystal, the output power of the VUV laser with photon energy 6.994 eV could be higher than 1 mW which is 1000 times higher than that of the synchrotron light source, and the bandwidth is still 0.26 meV. With a wider slit and pass energy used on the electron energy analyzer, the energy resolution of the spin resolved and momentum resolved system could be better than 20 meV which is not only far better than former spin resolved system but also the system has good momentum resolution.

Based on the experience of developing the VUV laser ARPES system, we designed a spin resolved ARPES system equipped with a powerful VUV laser, and the 3D model of the system is shown in Fig. 2.17.

In addition to the spin resolved detector, a self designed ultra low temperature cryostat with four-axes of freedom (polar angle rotation and translational motion along X, Y and Z axes) is equipped on the system. As shown in Fig. 2.17, the four axes cryostat is mounted on one side of the modified mu-metal analysis cham-

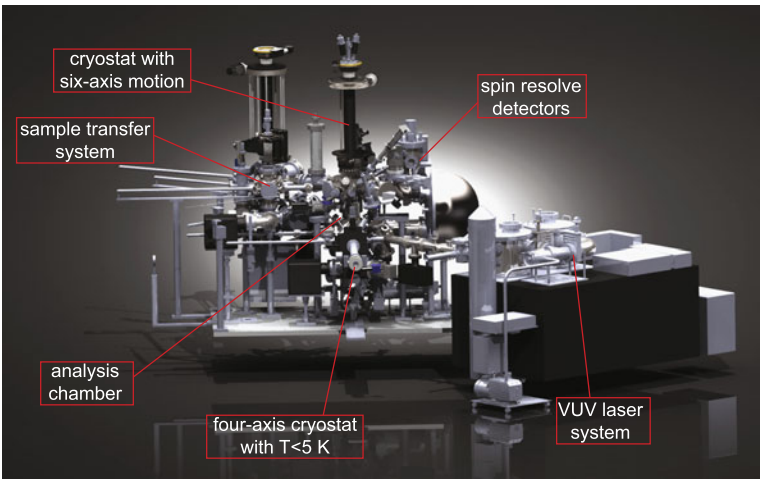

Fig. 2.17 The 3D model of spin resolved ARPES system

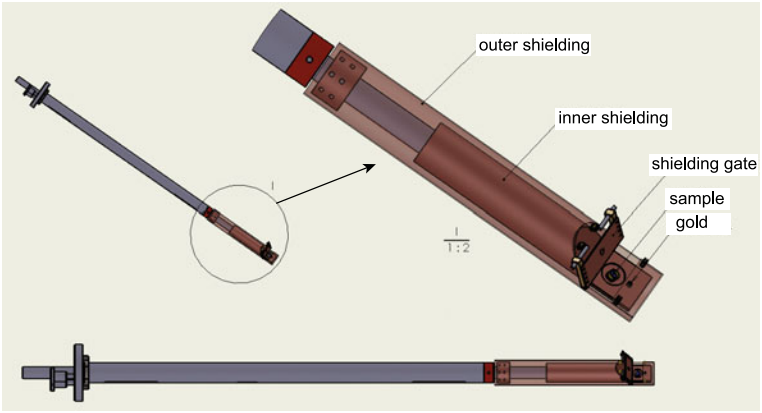

Fig. 2.18 The 3D model of the 4 axes cryostat

ber. The 3D model of the four axes cryostat is shown in Fig. 2.18. The cryostat is cooled by flowing liquid helium, and the temperature of cold-tip (the product of Janis) could be lower than 1.8 K by pumping with a mechanical vacuum pump. On the sample block, a sample position and a piece of gold are designed, and the temperature of the sample block is expected to be below 5 K. Actually, by our test, the temperature at sample position could be lower than 3 K. With such design and such low temperature at sample position, many materials with interesting physical properties at low temperature below 10 K could be studied, but it's difficult for a 6 axes cryostat with minimum temperature 12 K. Moreover, the piece of gold mounted on the sample block brings us the possibility of examining the Fermi level at any time

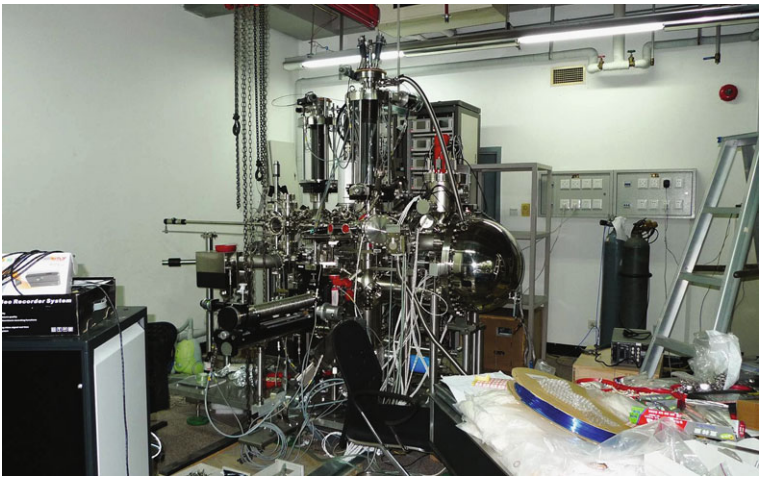

Fig. 2.19 The photo of completed spin resolved ARPES system

during the experiments. Moreover, a six-axes cryostat is equipped on the top of the mu-metal analysis chamber, and the two cryostats will be a complement of each other.

With the design shown in Fig. 2.17, the installation of the spin resolved ARPES system is completed (Fig. 2.19). The test result of the energy resolution is better than 5 meV which is far better than nowadays spin resolved ARPES system (with and energy resolution usually ~100 meV).

Combined with a high photon flux VUV laser (6.994 eV), the newly developed system gave a new record of energy resolution (better than 5 meV) of spin resolved ARPES systems in the world [39–43]. In addition, two individual cryostats including one six-axes (minimum temperature 12 K) and another four-axes (minimum temperature <5 K) are equipped on the system. To enrich the type of photon energy, a gas discharge lamp (SPECS) is also equipped on the system, and the lamp could work with He, Ne, Ar, and Xe gas which will produce more types of photon energy than only He. On the mu-metal analysis chamber, an x-ray source with Mg and Al targets which could produce x-ray with photon energy 1253 eV and 1486.994 eV is equipped to perform regular x-ray photoemission (XPS) experiments. Moreover, there is a molecular beam epitaxy system (MBE) used for film growth and surface treatment directly connected to the analysis chambers, and the prepared sample in this chamber could be transferred into the analysis chamber to perform photoemission experiments in situ. Combined with the MBE chamber, a scanning tunneling microscope (STM) is used to characterize the surface of samples.

It's worth mentioning that a polarizer which could tune the polarization of the 6.994 eV photons is mounted on the VUV laser system. The matrix element effect in ARPES experiments induced by photon polarization could be studied by using such a polarizer.

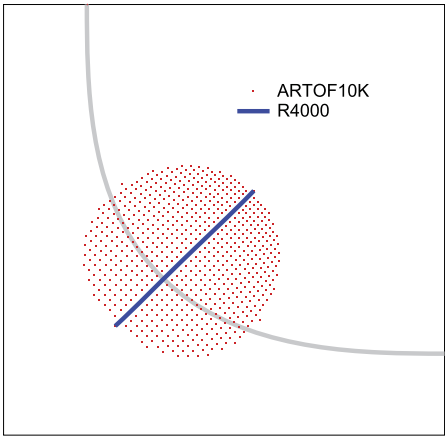

Fig. 2.20 Comparison of the momentum cut in Brillouin zone between time-of-flight and hemisphere energy analyzer

2.4.2 The Development of Time-of-Flight ARPES System

As the development of new techniques, a new generation of electron energy analyzer is introduced into the photoemission field, based on measuring the time of electrons flying from the sample to the detector. ARTOF10K, a product of Scienta is such a kind of electron energy analyzer which could detect the photon electrons in a solid angle with momentum resolution, while the hemispherical energy analyzer R4000 only probes the electrons in a plane angle. As the momentum cuts shown in Fig. 2.20, the hemispherical energy analyzer only gives a line momentum cut in the Brillouin zone while the ARTOF10K analyzer gives a plane momentum cut. The efficiency of angular detection is improved by ∼250 times, by using the new analyzer. Based on the new analyzer and our VUV laser, a time-of-flight ARPES system is developed in our lab.

By reason of measuring the flying time of electrons to calculate the energy of electrons, the time-of-flight analyzer should be equipped with a pulse light source, and one measurement should be completed between two adjacent pulses. So, the gas discharge lamp which produces continuous photons isn't compatible with the new analyzer. Laser with pulse characteristics is a perfect light source for such an analyzer. The photon energy of the second harmonic light after KBBF is 6.994 eV, the work function of solid materials is around 4∼5 eV, so the energy of outgoing electrons is about 2∼3 eV, and the distance from sample to detector is ∼1 m. With simple calculation, the flying time of electrons from sample to detector is about 1 μs, so the repetition frequency of the laser should be less than 1 MHZ. A 1 MHZ pump laser with wavelength 355 nm is adopted to produce 177 nm VUV laser after KBBF. Because of the reduced repetition frequency compared to the 80 MHZ pump laser used on the regular VUV laser-based ARPES system, to preserve the count rate, the photon flux in per pulse should be enhanced. A pump laser with the same average pump power as using in the VUV laser-based ARPES system will grantee the average photon flux comparable with the 80 MHZ laser system.

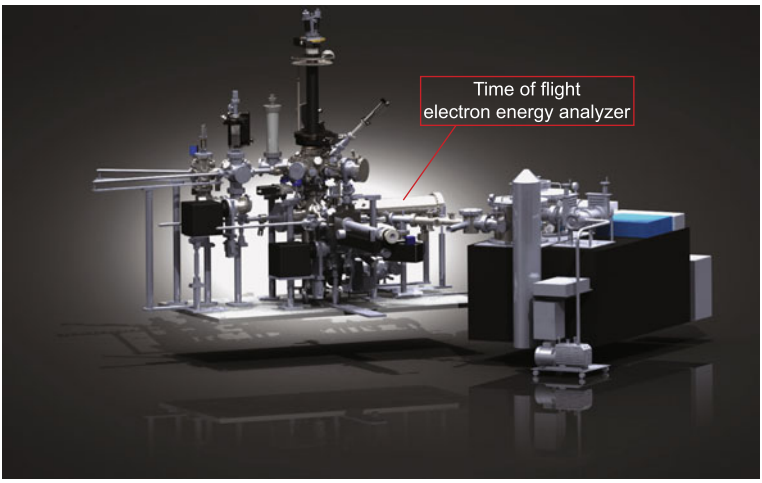

Fig. 2.21 The 3D model of the time-of-flight ARPES system

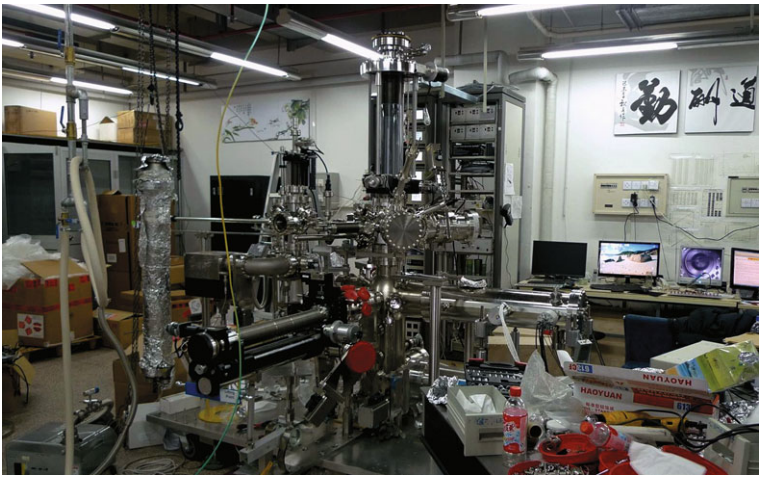

Fig. 2.22 The completed time-of-flight ARPES system

Figure 2.21 shows the time-of-flight ARPES system. Similar to the spin resolved ARPES system, two cryostats with six- and four-axes freedom are designed on the time-of-flight system. The low temperature of cryostat will make it possible to take advantage of the high resolution of a time-of-flight electron energy analyzer.

Figure 2.22 shows the completed time-of-flight ARPES system which is under testing.

The expected energy resolution of the time-of-flight ARPES system should be at the scale of 10^{-1} meV. With two-dimensional detector, the angular resolution will be improved to be better than 0.08°. The system also has a large detection angle

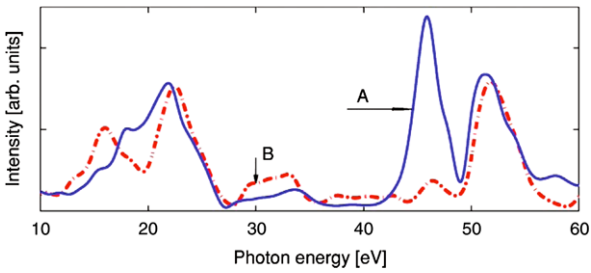

Fig. 2.23 The calculation of matrix element effect in Bi2212. Reprinted with permission from [47], copyright 2004, American Physical Society

with $\pm 18°$ from the specs of the ARTOF10K analyzer. Similar to the application of hemispherical energy analyzer in history (one-dimensional detection in momentum space), the new ARPES system equipped with a time-of-flight electron energy analyzer (two-dimensional detection) will bring a new leap in photoemission experiments.

2.4.3 Tunable Laser-Based ARPES System

In photoemission experiments, the matrix element effect $|M_{f,i}^{\mathbf{k}}|^2$ is a function of photon energy. Special photon energy may only probe special bands in materials. Taking high-temperature superconductor Bi2212 for an example, only anti-bonding band could be resolved by 6.994 eV laser for our current polarization and experimental setup. But when the photon energy is 7.5 eV which is only 504 meV higher than 6.994 eV, both the bonding and antibonding band could be observed [44]. First-principles calculations in Bi2212 give a photon energy dependence of spectral weight for the bonding and antibonding band, as shown in Fig. 2.23 [45–47]. It's necessary to develop a ARPES system with tunable photon energy avoiding missing some bands.

We have developed a tunable laser-based on the second harmonic generation from KBBF crystal with a tunable pump laser. This laser system will be equipped on the VUV laser ARPES system to overcome the possibility of missing some bands in materials because of single photon energy. The regular ARPES will have rich photon energies, including the 20.218 eV, 40.8 eV from helium discharge lamp, 6.994 eV from the VUV laser and 5.9∼7.09 eV from the tunable laser.

2.5 Summary

We have developed the first VUV laser-based ARPES system of which the energy resolution is improved to be better than 1 meV for the first time. Moreover, the photon flux of the VUV laser is two or three orders higher than the regular synchrotron light source and helium discharge lamp, and the bulk sensitivity is enhanced in the study of solid materials because of low photon energy.

Based on the improved VUV laser, we also developed a spin resolved ARPES system with energy resolution better than 5 meV which is far better than the regular spin resolved photoemission system. With special design, the newly developed spin resolved system could probe the full polarization of the electron beam. In addition, a MBE system and a STM are equipped to prepare films and characterize the surface of samples. We also designed a cryostat with four-axes freedom, and the temperature of the sample position could be lower than 3 K by pumping the flowing liquid helium.

With the developing of technique, we designed a time-of-flight ARPES system combined with the VUV laser. The electron energy analyzer ARTOF10K is a new product of Scienta with two-dimensional detection that could detect a momentum plane rather than a momentum line in the Brillouin zone. For this reason, expect for the much improved momentum resolution, the efficiency of detection is improved by 250 times higher than the hemisphere analyzer. A same cryostat with four axes as has been equipped on the spin resolved ARPES system will provide the possibility to measure samples under 5 K.

References

1. Chen, C., Lu, J., Togashi, T., Suganuma, T., Sekikawa, T., Watanabe, S., Xu, Z., Wang, J.: Second-harmonic generation from a $KBe_2BO_3F_2$ crystal in the deep ultraviolet. Opt. Lett. **27**(8), 637–639 (2002)
2. Liu, G., Wang, G., Zhu, Y., Zhang, H., Zhang, G., Wang, X., Zhou, Y., Zhang, W., Liu, H., Zhao, L., Meng, J., Dong, X., Chen, C., Xu, Z., Zhou, X.J.: Development of a vacuum ultraviolet laser-based angle-resolved photoemission system with a superhigh energy resolution better than 1 meV. Rev. Sci. Instrum. **79**(2), 023105 (2008)
3. Damascelli, A., Hussain, Z., Shen, Z.-X.: Angle-resolved photoemission studies of the cuprate superconductors. Rev. Mod. Phys. **75**, 473–541 (2003)
4. Hertz, H.: Ann. Phys. (Leipzig) **31**, 983 (1887)
5. Einstein, A.: Ann. Phys. (Leipzig) **31**, 132 (1905)
6. Randeria, M., Ding, H., Campuzano, J.-C., Bellman, A., Jennings, G., Yokoya, T., Takahashi, T., Katayama-Yoshida, H., Mochiku, T., Kadowaki, K.: Momentum distribution sum rule for angle-resolved photoemission. Phys. Rev. Lett. **74**, 4951–4954 (1995)
7. Gadzuk, J.W., Šunjić, M.: Excitation energy dependence of core-level x-ray-photoemission-spectra line shapes in metals. Phys. Rev. B **12**, 524–530 (1975)
8. Mahan, G.D.: Theory of photoemission in simple metals. Phys. Rev. B **2**, 4334–4350 (1970)
9. Schaich, W.L., Ashcroft, N.W.: Model calculations in the theory of photoemission. Phys. Rev. B **3**, 2452–2465 (1971)
10. Caroli, C., Lederer-Rozenblatt, D., Roulet, B., Saint-James, D.: Inelastic effects in photoemission: microscopic formulation and qualitative discussion. Phys. Rev. B **8**, 4552–4569 (1973)
11. Feibelman, P.J., Eastman, D.E.: Photoemission spectroscopy—correspondence between quantum theory and experimental phenomenology. Phys. Rev. B **10**, 4932–4947 (1974)
12. Fan, H.Y.: Theory of photoelectric emission from metals. Phys. Rev. **68**, 43–52 (1945)
13. Berglund, C.N., Spicer, W.E.: Photoemission studies of copper and silver: theory. Phys. Rev. **136**, A1030–A1044 (1964)
14. Hüfner, S.: Photoelectron Spectroscopy: Principles and Applications. Springer, Berlin Heidelberg, New York (1996)
15. Abrikosov, A.A., Gorkov, L.P., Dzialoshinskii, I.E.: Quantum Field Theoretical Methods in Statistical Physics. Pergamon, Elmsford (1965)

16. Hedin, L.: Solid State Physics: Advances in Research and Applications. Academic, New York (1969)
17. Mahan, G.D.: Quantum Theory of Many-Particle Systems. Plenum, New York (1981)
18. Rickayzen, G.: Green's Functions and Condensed Matter in Techniques of Physics, vol. 7. Academic, London (1991)
19. Seah, M.P., Dench, W.A.: Quantitative electron spectroscopy of surfaces: a standard data base for electron inelastic mean free paths in solids. Surf. Interface Anal. **1**(1), 2–11 (1979)
20. Sekiyama, A., Iwasaki, T., Matsuda, K., Saitoh, Y., Onuki, Y., Suga, S.: Probing bulk states of correlated electron systems by high-resolution resonance photoemission. Nature **403**(6768), 396–398 (2000)
21. Chen, C., Xu, Z., Deng, D., Zhang, J., Wong, G.K.L., Wu, B., Ye, N., Tang, D.: The vacuum ultraviolet phase-matching characteristics of nonlinear optical $KBe_2BO_3F_2$ crystal. Appl. Phys. Lett. **68**(21), 2930–2932 (1996)
22. Kanai, T., Kanda, T., Sekikawa, T., Watanabe, S., Togashi, T., Chen, C., Zhang, C., Xu, Z., Wang, J.: Generation of vacuum-ultraviolet light below 160 nm in a KBBF crystal by the fifth harmonic of a single-mode Ti:sapphire laser. J. Opt. Soc. Am. B **21**(2), 370–375 (2004)
23. Togashi, T., Kanai, T., Sekikawa, T., Watanabe, S., Chen, C., Zhang, C., Xu, Z., Wang, J.: Generation of vacuum-ultraviolet light by an optically contacted, prism-coupled $KBe_2BO_3F_2$ crystal. Opt. Lett. **28**(4), 254–256 (2003)
24. Kiss, T., Kanetaka, F., Yokoya, T., Shimojima, T., Kanai, K., Shin, S., Onuki, Y., Togashi, T., Zhang, C., Chen, C.T., Watanabe, S.: Photoemission spectroscopic evidence of gap anisotropy in an f-electron superconductor. Phys. Rev. Lett. **94**, 057001 (2005)
25. Kiss, T., Shimojima, T., Kanetaka, F., Kanai, K., Yokoya, T., Shin, S., Onuki, Y., Togashi, T., Zhang, C.Q., Chen, C.T., Watanabe, S.: Ultrahigh-resolution photoemission spectroscopy of superconductors using a VUV laser. J. Electron Spectrosc. Relat. Phenom. **144–147**, 953–956 (2005)
26. Koralek, J.D., Douglas, J.F., Plumb, N.C., Sun, Z., Fedorov, A.V., Murnane, M.M., Kapteyn, H.C., Cundiff, S.T., Aiura, Y., Oka, K., Eisaki, H., Dessau, D.S.: Laser based angle-resolved photoemission, the sudden approximation, and quasiparticle-like spectral peaks in $Bi_2Sr_2CaCu_2O_{8+\delta}$. Phys. Rev. Lett. **96**, 017005 (2006)
27. Koralek, J.D., Douglas, J.F., Plumb, N.C., Griffith, J.D., Cundiff, S.T., Kapteyn, H.C., Murnane, M.M., Dessau, D.S.: Experimental setup for low-energy laser-based angle resolved photoemission spectroscopy. Rev. Sci. Instrum. **78**(5), 053905 (2007)
28. Yamasaki, T., Yamazaki, K., Ino, A., Arita, M., Namatame, H., Taniguchi, M., Fujimori, A., Shen, Z.-X., Ishikado, M., Uchida, S.: Unmasking the nodal quasiparticle dynamics in cuprate superconductors using low-energy photoemission. Phys. Rev. B **75**, 140513 (2007)
29. Zhou, X.J., Wannberg, B., Yang, W.L., Brouet, V., Sun, Z., Douglas, J.F., Dessau, D., Hussain, Z., Shen, Z.X.: Space charge effect and mirror charge effect in photoemission spectroscopy. J. Electron Spectrosc. Relat. Phenom. **142**(1), 27–38 (2005)
30. Kisker, E., Clauberg, R., Gudat, W.: Electron spectrometer for spin-polarized angle- and energy-resolved photoemission from ferromagnets. Rev. Sci. Instrum. **53**(8), 1137–1144 (1982)
31. Gray, L.G., Hart, M.W., Dunning, F.B., Walters, G.K.: Simple, compact, medium-energy Mott polarization analyzer. Rev. Sci. Instrum. **55**(1), 88–91 (1984)
32. Raue, R., Hopster, H., Kisker, E.: High-resolution spectrometer for spin-polarized electron spectroscopies of ferromagnetic materials. Rev. Sci. Instrum. **55**(3), 383–388 (1984)
33. Tang, F.-C., Zhang, X., Dunning, F.B., Walters, G.K.: Compact low-energy Mott polarimeter for use in energy- and angle-resolved polarization studies. Rev. Sci. Instrum. **59**(3), 504–505 (1988)
34. Gay, T.J., Dunning, F.B.: Mott electron polarimetry. Rev. Sci. Instrum. **63**(2), 1635–1651 (1992)
35. Huang, D.-J., Lee, J.-Y., Suen, J.-S., Mulhollan, G.A., Andrews, A.B., Erskine, J.L.: Adapting a compact Mott spin polarimeter to a large commercial electron energy analyzer for spin-polarized electron spectroscopy. Rev. Sci. Instrum. **64**(12), 3474–3479 (1993)

36. Burnett, G.C., Monroe, T.J., Dunning, F.B.: High-efficiency retarding-potential Mott polarization analyzer. Rev. Sci. Instrum. **65**(6), 1893–1896 (1994)
37. Petrov, V.N., Landolt, M., Galaktionov, M.S., Yushenkov, B.V.: A new compact 60 kV Mott polarimeter for spin polarized electron spectroscopy. Rev. Sci. Instrum. **68**(12), 4385–4389 (1997)
38. Getzlaff, M., Heidemann, B., Bansmann, J., Westphal, C., Schonhense, G.: A variable-angle electron spin polarization detection system. Rev. Sci. Instrum. **69**(11), 3913–3923 (1998)
39. Ghiringhelli, G., Larsson, K., Brookes, N.B.: High-efficiency spin-resolved and spin-integrated electron detection: parallel mounting on a hemispherical analyzer. Rev. Sci. Instrum. **70**(11), 4225–4230 (1999)
40. Huang, D.J., Wu, W.P., Chen, J., Chang, C.F., Chung, S.C., Yuri, M., Lin, H.-J., Johnson, P.D., Chen, C.T.: Performance of a Mott detector for undulator-based spin-resolved spectroscopy. Rev. Sci. Instrum. **73**(11), 3778–3783 (2002)
41. Souma, S., Takayama, A., Sugawara, K., Sato, T., Takahashi, T.: Ultrahigh-resolution spin-resolved photoemission spectrometer with a mini Mott detector. Rev. Sci. Instrum. **81**(9), 095101 (2010)
42. Jozwiak, C., Graf, J., Lebedev, G., Andresen, N., Schmid, A.K., Fedorov, A.V., El Gabaly, F., Wan, W., Lanzara, A., Hussain, Z.: A high-efficiency spin-resolved photoemission spectrometer combining time-of-flight spectroscopy with exchange-scattering polarimetry. Rev. Sci. Instrum. **81**(5), 053904 (2010)
43. Okuda, T., Miyamaoto, K., Miyahara, H., Kuroda, K., Kimura, A., Namatame, H., Taniguchi, M.: Efficient spin resolved spectroscopy observation machine at Hiroshima Synchrotron Radiation Center. Rev. Sci. Instrum. **82**(10), 103302 (2011)
44. Iwasawa, H., Douglas, J.F., Sato, K., Masui, T., Yoshida, Y., Sun, Z., Eisaki, H., Bando, H., Ino, A., Arita, M., Shimada, K., Namatame, H., Taniguchi, M., Tajima, S., Uchida, S., Saitoh, T., Dessau, D.S., Aiura, Y.: Isotopic fingerprint of electron-phonon coupling in high-T_c cuprates. Phys. Rev. Lett. **101**, 157005 (2008)
45. Bansil, A., Lindroos, M.: Importance of matrix elements in the ARPES spectra of BISCO. Phys. Rev. Lett. **83**, 5154–5157 (1999)
46. Lindroos, M., Sahrakorpi, S., Bansil, A.: Matrix element effects in angle-resolved photoemission from $Bi_2Sr_2CaCu_2O_8$: energy and polarization dependencies, final state spectrum, spectral signatures of specific transitions, and related issues. Phys. Rev. B **65**, 054514 (2002)
47. Chuang, Y.-D., Gromko, A.D., Fedorov, A.V., Aiura, Y., Oka, K., Ando, Y., Lindroos, M., Markiewicz, R.S., Bansil, A., Dessau, D.S.: Bilayer splitting and coherence effects in optimal and underdoped $Bi_2Sr_2CaCu_2O_{8+\delta}$. Phys. Rev. B **69**, 094515 (2004)

http://www.springer.com/978-3-642-32471-0

Photoemission Spectroscopy on High Temperature Superconductor
A Study of Bi2Sr2CaCu2O8 by Laser-Based Angle-Resolved Photoemission

Zhang, W.

2013, XVI, 140 p., Hardcover
ISBN: 978-3-642-32471-0